# CD11b+Ly6C++Ly6G− CELLS WITH SUPPRESSIVE ACTIVITY TOWARDS T CELLS ACCUMULATE IN LUNGS OF INFLUENZA A VIRUS-INFECTED MICE

**P. Milanez-Almeida[1,+], T. Ulas[2], M. Pasztoi[1], S. Glage[3], K. Schughart[4], M. B. Lutz[5], J. L. Schultze[2], J. Huehn[1,\*]**

[1] Department of Experimental Immunology, Helmholtz Centre for Infection Research, Braunschweig, Germany
[2] Genomics and Immunoregulation, LIMES – Institute, University of Bonn, Bonn, Germany
[3] Institute for Laboratory Animal Science, Hannover Medical School, Hannover, Germany
[4] Department of Infection Genetics, Helmholtz Centre for Infection Research, Braunschweig, Germany, University of Veterinary Medicine Hannover, University of Tennessee Health Science Center, Memphis, USA
[5] Institute of Virology and Immunobiology, University of Würzburg, Würzburg, Germany

Influenza A virus (IAV) infection causes an acute respiratory disease characterized by a strong inflammatory immune response and severe immunopathology. Proinflammatory mechanisms are well described in the murine IAV infection model, but less is known about the mechanisms leading to the resolution of inflammation. Here, we analyzed the contribution of CD11b+Ly6C++Ly6G− cells to this process. An accumulation of CD11b+Ly6C++Ly6G− cells within the lungs was observed during the course of IAV infection. Phenotypic characterization of these CD11b+Ly6C++Ly6G− cells by flow cytometry and RNA-Seq revealed an activated phenotype showing both pro- and anti-inflammatory features, including the expression of inducible nitric oxide synthase (iNOS) by a fraction of cells in an IFN-γ-dependent manner. Moreover, CD11b+Ly6C++Ly6G− cells isolated from lungs of IAV-infected animals displayed suppressive activity when tested *in vitro,* and iNOS inhibitors could abrogate this suppressive activity. Collectively, our data suggest that during IAV infection, CD11b+Ly6C++Ly6G− cells acquire immunoregulatory function, which might contribute to the prevention of pathology during this life-threatening disease.

**Keywords:** monocytes, inducible nitric oxide synthase, influenza A virus, infection, immunosuppression

## Introduction

Immune regulation is especially important in the context of an acute infection of the respiratory tract with influenza A virus (IAV), since lethality here is caused by inflammation-induced lung destruction [1, 2]. Different immune mechanisms counter IAV infection while assuring tissue integrity in the delicate environment of lungs. IL-10 production by effector T cells, for example, is essential for mice to maintain immune balance and evade lung immunopathology although efficiently clearing the virus [3]. Foxp3-expressing regulatory T cells (Treg cells) also play a role during the immune response to IAV, since virus-specific Foxp3+ Treg cells vigorously increase at the site of infection, control cytotoxic T cell-mediated lung inflammation during secondary infections [4, 5], and promote recovery [6]. Notably, lethal IAV infection in mice

is attenuated if the number of monocyte-derived cells, which are myeloid cells phenotypically characterized as CD11b+Ly6C++Ly6G−, is reduced [7, 8]. In fact, upon IAV infection, monocyte-derived CD11b+Ly6C++Ly6G− cells can differentiate into tumor necrosis factor-α (TNF-α)/ inducible nitric oxide synthase (iNOS)-producing dendritic cells (TiP-DC), which contribute to the induction of potent CD8+ T cell responses and severe lung inflammation [9, 10]. However, CD11b+Ly6C++Ly6G− cells are known to react to different stimuli with a remarkable plasticity, being even able to give rise to cell populations showing immunosuppressive activity, such as for example myeloid-derived suppressor cells [11, 12]. Suppressive CD11b+Ly6C++Ly6G− cells can dampen T cell responses via different mechanisms, including tyrosine nitration of the T cell receptor [13] and local depletion of tryptophan by the activity of indoleamine 2,3-dioxygenase (IDO) [14,

* Corresponding author: Jochen Huehn; Inhoffenstraße 7, 38124 Braunschweig, Germany; Phone: +49 531 6181 3310; Fax: +49 531 6181 3399; E-mail: Jochen.Huehn@helmholtz-hzi.de

+ Present address: Laboratory of Systems Biology, National Institute of Health, Bethesda, USA

15]. Immunosuppressive monocyte-derived cells can also restrain T cell responses via consumption of arginine and production of reactive nitrogen and oxygen species by iNOS and arginase-1 (Arg1) expression [11].

Although first experimental data suggested a role of immunosuppressive myeloid cells during IAV infection [16, 17], the importance of this cell type for the prevention of inflammation-induced lung destruction is only incompletely understood. Thus, we here hypothesized that monocyte-derived cells can acquire an anti-inflammatory phenotype in lungs of IAV-infected mice to suppress an exaggerated T cell response. To test this, we sublethally infected mice with a mouse-adapted IAV strain, isolated CD11b$^+$Ly6C$^{++}$Ly6G$^-$ cells from infected lungs, and characterized their phenotype and function. We observed that *ex vivo* isolated CD11b$^+$Ly6C$^{++}$Ly6G$^-$ cells from IAV-infected mice displayed a dual pro- and anti-inflammatory phenotype and were able to suppress naive T cell proliferation *in vitro*. Suppressive activity was dependent on iNOS but not on Arg1 or IDO. Furthermore, *in vivo* iNOS expression was under control of IFN-γ. In summary, our data suggest that CD11b$^+$Ly6C$^{++}$Ly6G$^-$ cells with an immunoregulatory phenotype accumulate in lungs of IAV-infected mice and might contribute to the local prevention of immunopathology. Thus, the functional role of monocytes and their progeny during IAV infection needs to be redefined.

## Materials and methods

### Mice

Wildtype C57BL/6JRj mice were either purchased from Janvier or bred at the Helmholtz Centre for Infection Research (Braunschweig, Germany). Female animals at age of 10 to 14 weeks were used. All mice were housed and handled under specific pathogen-free conditions in accordance with good animal practice as defined by FELASA and the national animal welfare body GV-SOLAS under supervision of the institutional animal welfare officer. Animal experiments were performed in accordance with institutional, state, and federal guidelines. The animal protocol was approved by the Niedersächsisches Landesamt für Verbraucherschutz und Lebensmittelsicherheit: animal licensing committee permission no. 33.14-42502-04-091/09. Animals were handled with appropriate care and welfare, and all efforts were made to minimize suffering.

### Virus preparation and mouse infection

Mouse-adapted influenza A/Puerto Rico/8/34 (H1N1 PR8 Münster) virus strain was produced as described before [18]. Intranasal infection was performed with one tenth of the median lethal dose (LD$_{50}$) as defined before for the respective virus batch ($2 \times 10^4$ focus forming viral units/mouse in 20 μl phosphate-buffered saline [PBS]) [19]. Mice were anaesthetized prior to infection by i.p. injec-

tion of 10 mg/ml ketamine and 1 mg/ml xylazine diluted in PBS (10 μl/g of body weight). Ophthalmic ointment was applied to prevent drying of the corneas, and mice were kept insulated to avoid loss of body heat. Health status and body weight were checked every second day. Intranasal infection resulted in rapid loss of body weight, reaching lowest levels between day 6 and day 8. Mice losing more than 20% of body weight within 2 days were euthanized, and the infection was considered lethal. I.p. injection of 1 mg of either anti-IFN-γ (R4-6A2) or rat IgG isotype control (HRPN) antibodies from BioXCell was performed on day 5 post infection (p.i.). Mice were sacrificed at indicated time points, and cells from spleen and lungs were isolated and analyzed.

### Histology

At day 14 of infection, IAV-infected animals were sacrificed and the lungs were excised, gently instilled, and subsequently fixed in 4% buffered formalin (pH 7.2). After trimming according to the Registry of Industrial Toxicology Animal-data recommendations [20] and dehydration (Shandon Hypercenter), the lungs were embedded in paraffin. Sections were deparaffinized with xylene and stained with H&E to evaluate general morphology by light microscopy (Axioskop 40, Zeiss). A blinded, semiquantitative scoring system was used to grade the pathologic changes in the lungs, as described previously [21].

### Organ isolation and preparation of single cell suspensions

Mice were sacrificed by CO$_2$ asphyxia, and spleen and PBS-perfused lungs were taken. Lungs were minced and digested at 37 °C for a total of 45 min in Iscove's Modified Dulbecco's Medium (Invitrogen), 10% fetal calf serum (Sigma-Aldrich), 0.2 mg/ml collagenase D (Roche), and 10 mg/ml DNAse (Roche). For the last 15 min of digestion, 0.8 U/ml Dispase (Roche) was added. Lung digestion was stopped by adding EDTA to a final concentration of 5 mM and by keeping samples on ice. Single cell suspensions were prepared by mechanical squeezing of minced spleens or digested lungs through 100 μm nylon meshes. Erythrocytes in spleen and lung samples were lysed by incubation with ammonium–chloride–potassium (ACK) buffer for 4 min at room temperature. Lysis was stopped by diluting ACK buffer in a tenfold volume of PBS–bovine serum albumin (BSA). Centrifugation steps were performed at 4 °C and 450 *g* for 8 min. If not described otherwise, samples were subsequently maintained in PBS–BSA.

### Cell staining for flow cytometry

Dead cells were stained using LIVE/DEAD® fixable dead cell stain kit (Invitrogen) as described by the manufacturer.

Fluorochrome-coupled antibodies recognizing mouse CD3 (clone 145-2C11), CD4 (RM4-5), CD11b (M1/70), CD11c (N418), CD19 (MB19-1), CD25 (PC61.5), CD44 (IM7), CD49b (DX5), CD62L (MEL-14), CD86 (GL1), CD90.2 (53-2.1), iNOS (C-11), and MHCII (M5/114.15.2) were purchased from either BD Biosciences, BioLegend, eBioscience or Santa Cruz Biotechnology. Specific antibody staining was performed at 4 °C in the dark for 15 min (surface staining) or 30 min (intracellular staining using Foxp3/Transcription Factor Staining Buffer Set from eBioscience). Spleens were stained in a total volume of 100 μl, and lung samples in 200 μl. To reduce unspecific antibody binding, surface and intracellular staining were performed in the presence of anti-CD16/CD32 (2.4G2, BioXCell) antibodies and ChromPure rat IgG whole molecule (Jackson ImmunoResearch), respectively, and using predetermined optimal antibody dilutions. Carboxyfluorescein succinimidyl ester (CFSE, Invitrogen) staining (10 μM) was performed at $2 \times 10^7$ cells/ml of PBS for 2 min and 45 s at room temperature. Reaction was stopped by adding a tenfold volume of complete RPMI 1640 medium (Invitrogen) containing 10% fetal calf serum (cRPMI) followed by two washing steps.

### Flow cytometry

Flow cytometry data were acquired on a BD Fortessa, and cells were sorted with help of a FACSAria II, all using BD FACSDiva software (BD Biosciences). Data were analyzed by means of FlowJo software (Treestar, Ashland, OR, USA). Only living single cells were considered for further flow cytometry analysis. Absolute cell numbers were calculated using a BD Accuri C6 (BD Biosciences) flow cytometer, with data analysis being performed using CFlow Plus software (BD Biosciences) according to instructions by the manufacturer.

### Suppression assay

Naive CD4 T cells were pre-enriched from murine spleens by magnetic sorting using anti-CD4 microbeads (Miltenyi Biotec) labeling followed by positive selection using an autoMACS (Miltenyi Biotec), as described by the manufacturer. Pre-enrichment was followed by fluorescence-activated cell sorting (FACS) with the target cells having the phenotype of single $CD90.2^+CD4^+CD62L^{high}CD44^-CD25^-$ events. $2 \times 10^5$ CFSE-labeled naive $CD4^+$ T cells were incubated in cRPMI in 96-wells plates for 4 days at 37 °C, >95% humidity and 5% $CO_2$ in the presence or absence of plate-bound 0.5 μg/ml anti-CD3 and 0.1 μg/ml anti-CD28 antibodies (145-2C11 and 37.51, both from eBioscience). $CD3^-CD19^-CD49b^-CD11b^+Ly6C^{++}Ly6G^-$ cells from digested lungs of IAV-infected mice were FACS-sorted and added to the cultures. 500 μg/ml L-NMMA, 200 μM 1-MDT (both from Sigma-Aldrich), and 500 μg/ml NOR-NOHA (Merck) were used to block iNOS, IDO, and Arg1, respectively.

### Enzyme-linked immunosorbent assay (ELISA)

To determine IFN-γ levels within lungs of IAV-infected mice, lungs were isolated and stored in 1 ml sterile PBS at −70 °C until homogenized. For homogenization, samples were thawed, diluted in 4 ml sterile PBS containing cOmplete™ Protease Inhibitor Cocktail (Merck) and processed using a homogenizator. After centrifugation, supernatants were stored at −70 °C until measurement using the Mouse IFN-γ ELISA MAX Deluxe kit (BioLegend) following the instructions of the manufacturer.

### RNA-Seq

Total RNA was isolated from sorted cells with RNAeasy Plus mini kit (Qiagen). The quality and integrity of total RNA were controlled on Agilent Technologies 2100 Bioanalyzer (Agilent Technologies). Purification of mRNA was done using polyT oligo-attached magnetic beads. Following the purification, the mRNA was used for library preparation using ScriptSeq v2 Library preparation kit (Epicentre). The sequencing was carried out on HiSeq2500 (Illumina) using 100 bp paired-end sequencing.

### RNA-Seq preprocessing

After base calling and demultiplexing using CASAVA version 1.8, the 100 bp paired-end reads were aligned to the murine reference genome mm10 from UCSC by TopHat2 version v2.0.11 and Bowtie2 version 2.2.1 using the default parameters. This annotation included 15,222 unique transcript entries with genomic coordinates. After mapping of the reads to the genome, we imported them into Partek Genomics Suite (PGS) version 6.6 to calculate the number of reads mapped to each transcript against the RefSeq [22] mm10 annotation download on April 2014. These raw read counts were used as input for DESeq to calculate normalized signals for each transcript using the default parameters [23]. After DESeq normalization, the normalized read counts were imported back into PGS, floored by setting all read counts to at least a read count of 1 after batch-correction. Subsequent to flooring, all transcripts having a maximum overall group means lower than 10 were removed. After dismissing the low expressed transcripts, the data comprised of 11,034 transcripts. RNA-Seq data can be accessed under GSE62795.

### Data analysis

A one-way analysis of variance (ANOVA) model was performed to calculate differentially expressed genes between the conditions "infected lung", "infected spleen", and "non-infected spleen", as well as the 1000 most variably expressed genes within the whole dataset. Differentially expressed genes were defined by a fold change (FC) >2
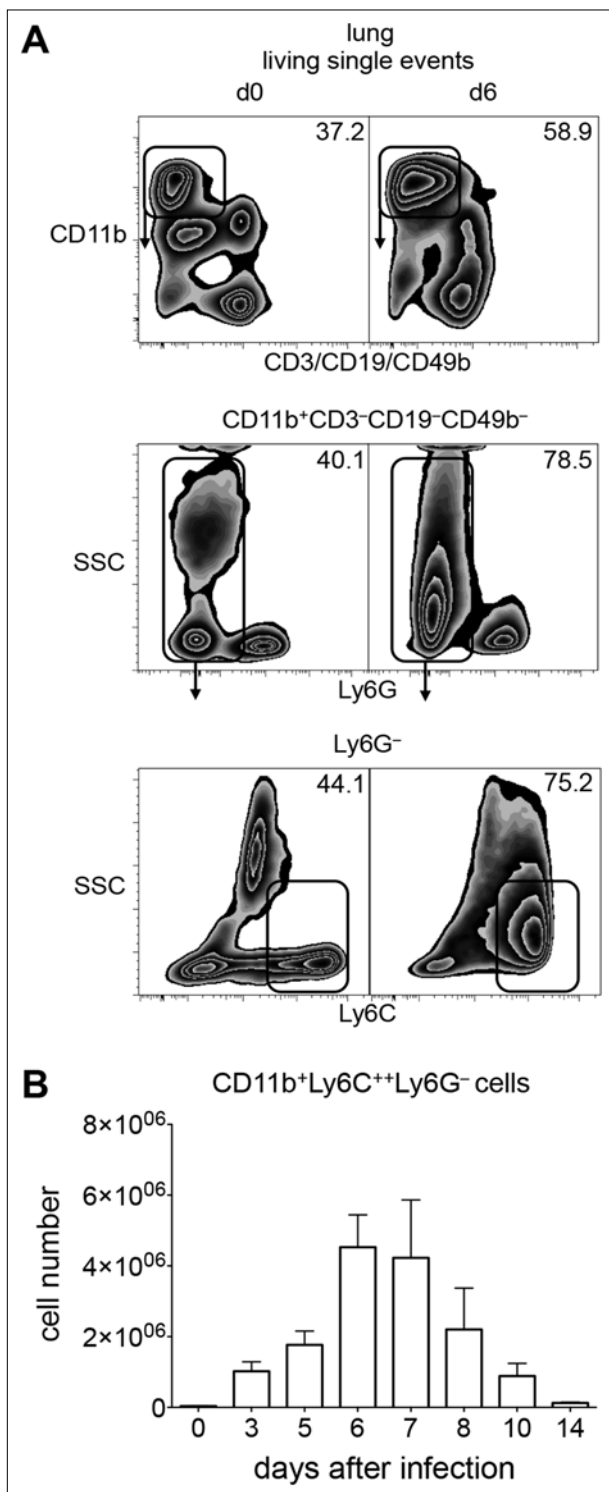
**Fig. 1.** CD11b$^+$Ly6C$^{++}$Ly6G$^-$ cells transiently accumulate in lungs of IAV-infected mice. (A) Gating strategy for CD11b$^+$Ly6C$^{++}$Ly6G$^-$ cells. Cells were isolated from lungs of PBS-treated mice (left, d0) or IAV-infected mice on day 6 p.i. (right, d6). Top panels were pregated on single events after exclusion of dead cells (see *Fig. S1*). Plots are representative for at least two independently performed experiments. Numbers indicate frequency of cells within gates. (B) Total number of CD11b$^+$Ly6C$^{++}$Ly6G$^-$ cells in lungs of PBS-treated (d0) or IAV-infected mice on indicated time points p.i. as determined by flow cytometry. Data were pooled from two independent experiments (mean ± SD, $n = 5$–13)

or ≤2, and a false discovery rate (FDR) corrected $p$-value < 0.05. To visualize the structure within the data, we performed principle component analysis (PCA) on all genes and hierarchical clustering (HC) on the 1000 most variable genes, with default settings in PGS, on $p$-values according to the expression values of the samples across the conditions.

The heat map of the $z$-scores of the log$_2$ expression profiles were generated using the Mayday open source software (http://www-ps.informatik.uni-tuebingen.de/mayday/ wp/) [24]. Gene ontology enrichment analysis (GOEA) was calculated for up- and down-regulated differentially expressed genes by BiNGO (http://www.psb.ugent.be/cbd/papers/BiNGO) [25, 26], which is implemented as a plugin for Cytoscape. For GOEA visualization, we used the Cytoscape plugins Enrichment Map (http://baderlab.org/Software/EnrichmentMap) [27] and WordCloud (http://baderlab.org/Software/WordCloud-Plugin) [28].

*Statistics*

GraphPad Prism software (La Jolla, CA, USA) was used to compare data applying two-tailed unpaired $t$ test with Welch's correction. $p$-values ≤ 0.05 were considered as statistically significant.

## Results

*Monocytic cells transiently accumulate in lungs of IAV-infected mice*

A number of different suppressive mechanisms were described to be essential for the prevention of immunopathology within the lungs during IAV infection. However, the contribution of monocyte-derived CD11b$^+$Ly6C$^{++}$Ly6G$^-$ cells is incompletely understood [16, 17]. Thus, here, we determined the changes within the myelomonocytic compartment from healthy to infected mice. Remarkable changes were observed within this population, which could be detected in the lungs of mice after infection with a sublethal dose of mouse-adapted H1N1 (PR8) virus strain (*Fig. 1A* and *S1*). In the early days after infection, CD11b$^+$Ly6C$^{++}$Ly6G$^-$ cell numbers steadily increased, achieving their highest levels on day 6 and day 7, but steadily decreasing afterwards *(Fig. 1B)*. At day 14, cell numbers returned to basal levels *(Fig. 1B)*. Next, we characterized the phenotype of CD11b$^+$Ly6C$^{++}$Ly6G$^-$ cells isolated from the lungs at the peak of their accumulation (i.e., day 6). In line with previous reports [7–9], a large fraction of these cells expressed CD11c or MHC class II, which are markers of differentiation of monocytes into dendritic cells *(Fig. 2)*. Furthermore, most cells isolated from infected lungs also expressed the activation marker CD86, suggesting that these cells are fully activated.
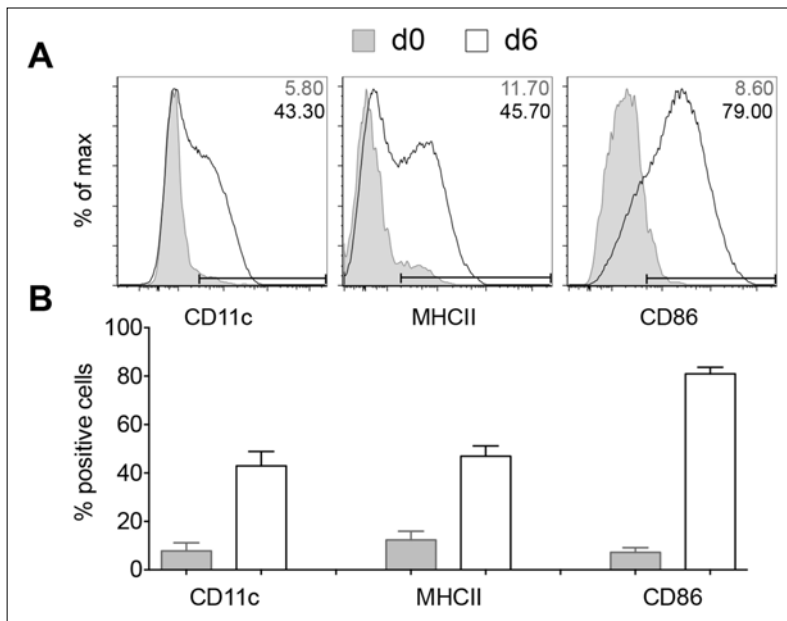
**Fig. 2.** CD11b^{+}Ly6C^{++}Ly6G^{−} cells in lungs of IAV-infected mice display an activated phenotype. (A) Histograms from representative mouse and (B) bar graph with pooled data show expression of CD11c, MHCII, and CD86 on CD11b^{+}Ly6C^{++}Ly6G^{−} cells. Cells were isolated from lungs of PBS-treated mice (gray) and IAV-treated mice on day 6 p.i. (black line) and analyzed by flow cytometry. Numbers in the histograms denote frequency of gated cells among total CD11b^{+}Ly6C^{++}Ly6G^{−} cells. Data derived from two independent experiments with a total of three (d0) or four mice (d6) are depicted
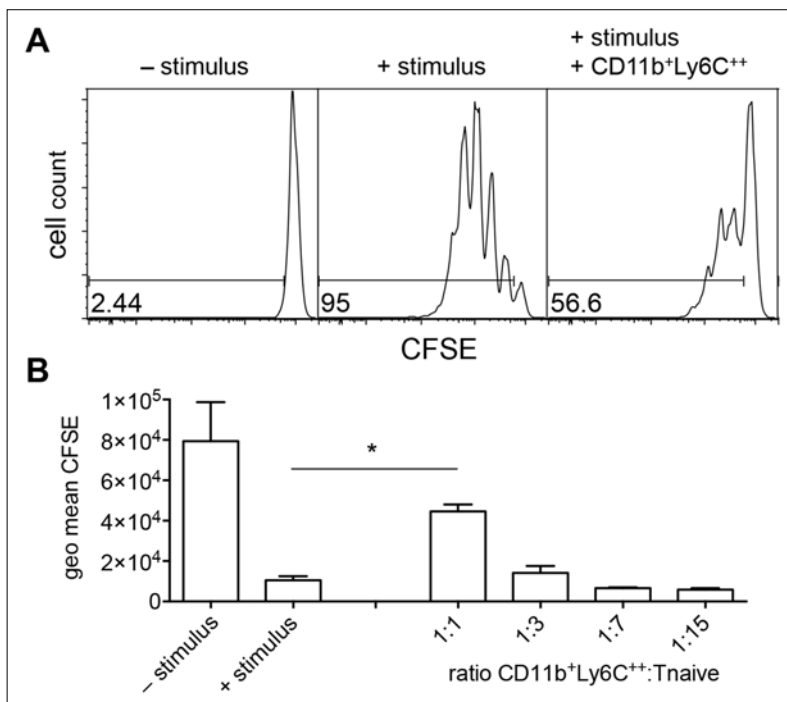
*CD11b^{+}Ly6C^{++}Ly6G^{−} cells isolated from lungs of IAV-infected mice display potent suppressive activity*

Since CD11b^{+}Ly6C^{++}Ly6G^{−} cells can also exert immunosuppression upon activation with different stimuli, we next examined the suppressive capacity of CD11b^{+}Ly6C^{++}Ly6G^{−} cells derived from IAV-infected lungs by performing a functional *in vitro* suppression assay. Naive CD4^{+} T cells were labeled with the proliferation dye CFSE and stimulated with plate-bound anti-CD3 and anti-CD28 antibodies, which leads to a significant proliferation (loss of CFSE) when compared to nonstimulated cells *(Fig. 3)*. When CD11b^{+}Ly6C^{++}Ly6G^{−} cells isolated from lungs of IAV-infected mice (day 6 p.i.) were added to the

cultures, proliferation of naive CD4^{+} T cells was efficiently inhibited *(Fig. 3)*, suggesting that CD11b^{+}Ly6C^{++}Ly6G^{−} cells isolated from the lungs of IAV-infected mice display suppressive activity.

*CD11b^{+}Ly6C^{++}Ly6G^{−} cells isolated from lungs of IAV-infected mice express both pro- and anti-inflammatory signature genes*

After having demonstrated a suppressive phenotype of CD11b^{+}Ly6C^{++}Ly6G^{−} cells isolated from lungs of IAV-infected mice, we next aimed to identify the molecular mechanism used by these cells to suppress immune re-



**Fig. 3.** CD11b^{+}Ly6C^{++}Ly6G^{−} cells isolated from lungs of IAV-infected mice suppress naive T cell proliferation. Naive CD4^{+} T cells were labeled with CFSE and stimulated for 4 days with plate-bound anti-CD3 and anti-CD28 antibodies (+stimulus) or left unstimulated (−stimulus) as control. CD11b^{+}Ly6C^{++}Ly6G^{−} cells isolated from lungs of IAV-infected mice (day 6) were added at a ratio of 1:1. At the end of the culture, cells were analyzed by flow cytometry. (A) Histograms show CFSE profile of naive CD4^{+} T cells pregated as living CD4^{+}CD11b^{−} cells. Numbers show frequency of cells that have lost CFSE. Each condition was performed in triplicates, and representative data from one out of two independently performed experiments are depicted. (B) Pooled geometric mean fluorescence intensity (geo mean) of CFSE in naive CD4^{+} T cells from the two experiments depicted in A (mean ± SD, n = 6). * = p ≤ 0.05, two-tailed unpaired t test with Welch's correction
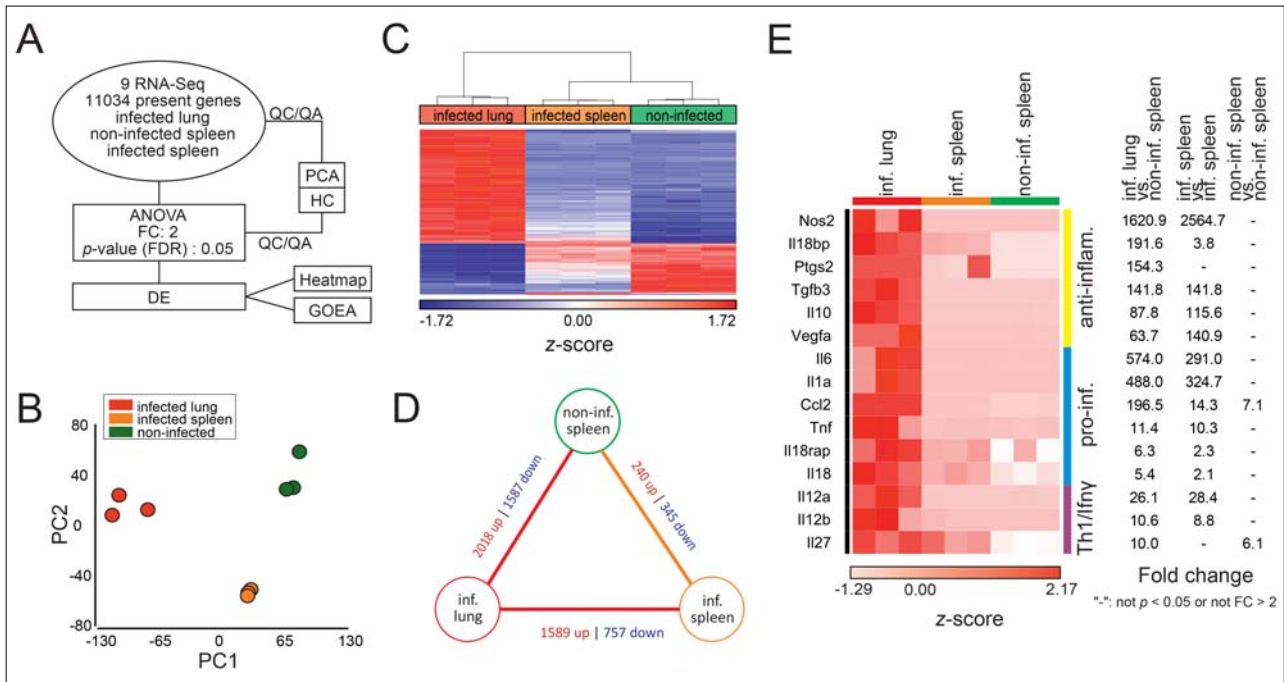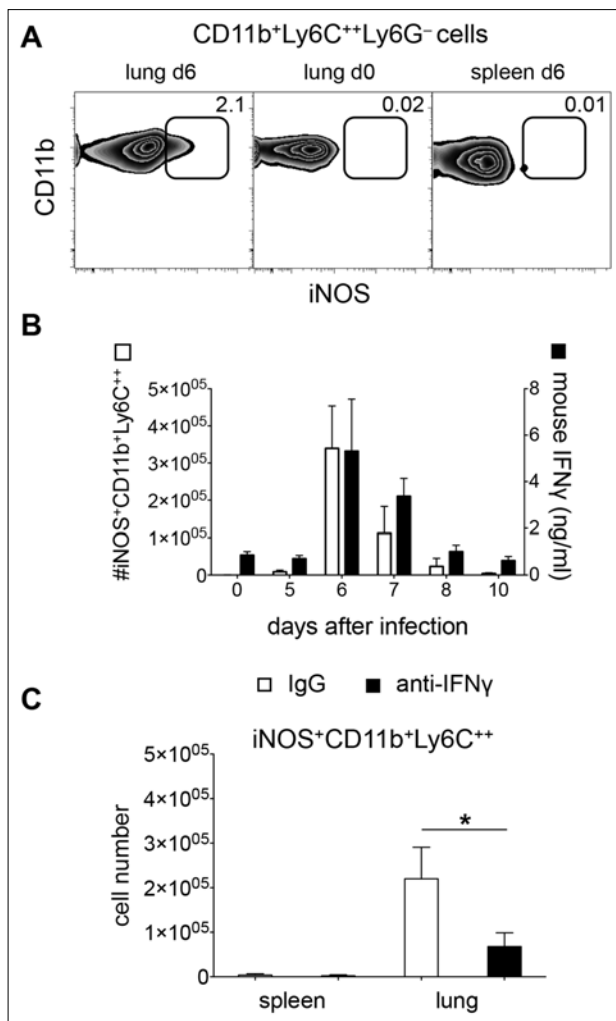
**Fig. 4.** CD11b⁺Ly6C⁺⁺Ly6G⁻ cells isolated from lungs of IAV-infected mice express both pro- and anti-inflammatory genes. (A) Schematic description of the RNA-Seq workflow. (B) Principal component analysis (PCA) using all 11,034 present transcripts was performed in Partek Genomics Suite (PGS) using default settings, and principle component 1 (PC1) and PC2 are plotted in a two-dimensional graph. Data were derived from three independently performed experiments. (C) Hierarchical clustering (HC) of 1000 transcripts with the most significant variance between "infected lung", "infected spleen", and "non-infected spleen". Standard settings for HC analysis in PGS to determine the source of variance in the dataset were used. (D) Visualization of differentially up and down regulated genes between all three experiments. (E) Heatmap (left) (standardized and scaled log₂ expression) of pro- and anti-inflammatory genes differentially expressed ($p$-value ≤ 0.05 and fold change ≥ 2) at least between "infected lung" and "non-infected spleen". Table (right) describes the fold changes between "infected lung" compared to "non-infected spleen", "infected lung" compared to "infected spleen" as well as "infected spleen" compared to "non-infected spleen". Fold changes which were between −2 and 2 or did not reach statistical significance by $p$-value ≤ 0.05 are represented by "–"

sponses. First, we analyzed the global transcriptome of FACS-sorted CD11b⁺Ly6C⁺⁺Ly6G⁻ cells isolated from lungs of mice on day 6 p.i. ("infected lung") by RNA-Seq, and CD11b⁺Ly6C⁺⁺Ly6G⁻ cells isolated from spleens of healthy mice ("non-infected spleen") or from spleens of mice on day 6 p.i. ("infected spleen") were taken as controls *(Fig. 4A)*. Unfortunately, we could not isolate sufficient numbers of CD11b⁺Ly6C⁺⁺Ly6G⁻ cells from non-infected lungs as additional control. An initial principle component analysis (PCA) using all 11,034 present transcripts revealed a clear separation of the three different cell populations for all three independently performed experiments *(Fig. 4B)*. Assessing and visualizing the variance in gene expression by hierarchical clustering (HC) of transcripts of the 1000 most variable genes within the dataset clearly showed strong differences between "infected lung" and the two groups "infected spleen" and "non-infected spleen," while a high degree of similarity was observed between "infected spleen" and "non-infected spleen." This finding was corroborated by the number of differentially expressed genes between "infected lung" vs. "infected spleen" (1589 up and 757 down) and between "infected lung" vs. "non-infected spleen" (2018 up and 1587 down), showing a higher transcriptional change when compared to a direct comparison of "infected spleen" vs. "non-in-

fected spleen" (240 up and 345 down) *(Fig. 4D)*. We also found that CD11b⁺Ly6C⁺⁺Ly6G⁻ cells isolated from the site of infection display a dual pro- and anti-inflammatory phenotype with an upregulation of mRNA transcripts for *Il1a, Il6, Il10, Il12a, Il12b, Il18, Il18bp, Il27, Tnf, Vegfa,* and *iNOS (Fig. 4E)*, while *Arg1* and *Ido1* did not show differential expression. In fact, *iNOS* was among the most upregulated genes in CD11b⁺Ly6C⁺⁺Ly6G⁻ cells from infected lungs when compared to corresponding cell populations isolated from spleens of healthy or infected mice, suggesting that iNOS might be functionally involved in the suppressive activity of lung-derived CD11b⁺Ly6C⁺⁺Ly6G⁻ cells.

To identify major biological processes altered in CD11b⁺Ly6C⁺⁺Ly6G⁻ cells during IAV infection, we performed gene ontology enrichment analyses (GOEA) followed by network visualization using the differentially expressed transcripts (2018 up and 1587 down) from "infected lung" vs. "non-infected spleen" *(Fig. S2)*. In this densely populated network, a significant number of network hubs defined by genes upregulated in "infected lung" (red edges and nodes) were linked to various pro-inflammatory processes like inflammatory response, response to oxygen species (ROS), apoptosis, and antigen presentation. At the same time, we observed an enrich-

**Fig. 5.** CD11b⁺Ly6C⁺⁺Ly6G⁻ cells in lungs of IAV-infected mice express iNOS in an IFN-γ-dependent manner. (A) Expression of iNOS by CD11b⁺Ly6C⁺⁺Ly6G⁻ cells from lungs of IAV-infected mice (lung d6), lungs of PBS-treated mice (lung d0), and spleens of IAV-infected mice (spleen d6) as determined by flow cytometry. Representative data from two independent experiments with a total of three (d0) or four mice (d6) are depicted. Numbers indicate frequency of cells within gates. (B) White bars: Total number of iNOS-producing CD11b⁺Ly6C⁺⁺Ly6G⁻ cells in lungs of PBS-treated (d0) and IAV-infected mice on indicated days p.i. Data were pooled from two independent experiments (mean ± SD, $n$ = 5–13). Black bars: Concentration of IFN-γ in lung homogenates of PBS-treated (d0) and IAV-infected mice on indicated days p.i. as determined by ELISA. Data were pooled from two independent infection experiments (mean ± SD, $n$ = 4–6) and were obtained from one ELISA experiment with each lung homogenate being measured in duplicates. (C) Total number of iNOS-producing CD11b⁺Ly6C⁺⁺Ly6G⁻ cells in lungs of IAV-infected mice on day 6 p.i. as determined by flow cytometry. One day before, mice were either injected with IgG isotype control (IgG, white bars) or anti-IFN-γ (aIFNγ, black bars) antibody. Data were pooled from two independent experiments (mean ± SD, $n$ = 5–7, * = $p \leq 0.05$, two-tailed unpaired $t$ test with Welch's correction)

inflammatory processes. Together, these data suggest that CD11b⁺Ly6C⁺⁺Ly6G⁻ cells isolated from lungs of IAV-infected mice show a dual pro- and anti-inflammatory phenotype, with a prominent expression of iNOS.

*CD11b⁺Ly6C⁺⁺Ly6G⁻ cells in lungs of IAV-infected mice express iNOS in an IFN-γ-dependent manner*

Flow cytometric analyses revealed that a small fraction of CD11b⁺Ly6C⁺⁺Ly6G⁻ cells isolated from IAV-infected lungs expressed iNOS (4.37 ± 1.88% [mean ± SD], $n$ = 4), while hardly any iNOS⁺CD11b⁺Ly6C⁺⁺Ly6G⁻ cells could be detected in lungs of healthy mice or spleens of infected mice *(Fig. 5A)*. Interestingly, iNOS⁺CD11b⁺Ly6C⁺⁺Ly6G⁻ cells appeared in lungs of IAV-infected mice on day 6 p.i. in a very transient manner, a phenotype that largely correlated with the local presence of IFN-γ *(Fig. 5B)*, known as potent inducer of iNOS [29]. Indeed, *in vivo* administration of neutralizing anti-IFN-γ antibodies led to a significant decrease in the number of iNOS⁺CD11b⁺Ly6C⁺⁺Ly6G⁻ cells in lungs of IAV-infected mice when compared to mice receiving isotype control antibodies *(Fig. 5C)*, although the overall outcome of disease was not altered by this treatment *(Fig. S3)*. These data suggest a direct link between IFN-γ expression and iNOS induction in CD11b⁺Ly6C⁺⁺Ly6G⁻ cells from lungs of IAV-infected mice.

*Suppressive capacity of CD11b⁺Ly6C⁺⁺Ly6G⁻ cells from IAV-infected lungs relies on iNOS activity*

Having shown that iNOS is expressed in a fraction of CD11b⁺Ly6C⁺⁺Ly6G⁻ cells derived from lungs of IAV-infected mice, we next asked if this enzyme mediates the suppressive capacity of these cells. In addition to iNOS, whose activity was blocked by addition of L-NMMA [30], we also tested the functional importance of Arg1 and IDO enzymes by addition of NOR-NOHA [31] and 1-MDT [32], respectively, since both enzymes were described to contribute to T cell suppression by myeloid cells in different settings [11, 12]. Stimulation of CFSE-labeled naive CD4⁺ T cells with plate-bound anti-CD3 and anti-CD28 antibodies resulted in strong T cell proliferation, which was not affected upon addition of chemical inhibitors *(Fig. 6A, upper row)*. As expected, addition of CD11b⁺Ly6C⁺⁺Ly6G⁻ cells isolated from lungs of IAV-infected mice at a ratio of 1:1 efficiently inhibited T cell proliferation *(Fig. 6A, lower row)*. Interestingly, this strong suppressive activity of lung-derived CD11b⁺Ly6C⁺⁺Ly6G⁻ cells was not affected by inhibition of Arg1 and IDO; however, addition of the iNOS inhibitor L-NMMA completely abrogated the inhibition of T cell proliferation *(Fig. 6)*. Hence, the data presented here show for the first time that CD11b⁺Ly6C⁺⁺Ly6G⁻ cells accumulating in lungs of IAV-infected mice display suppressive capacity that relies on the enzymatic activity of iNOS.

ment of processes like phagocytosis, positive regulation of angiogenesis, wound healing, and lung alveolus development, which are all known to be associated with anti-
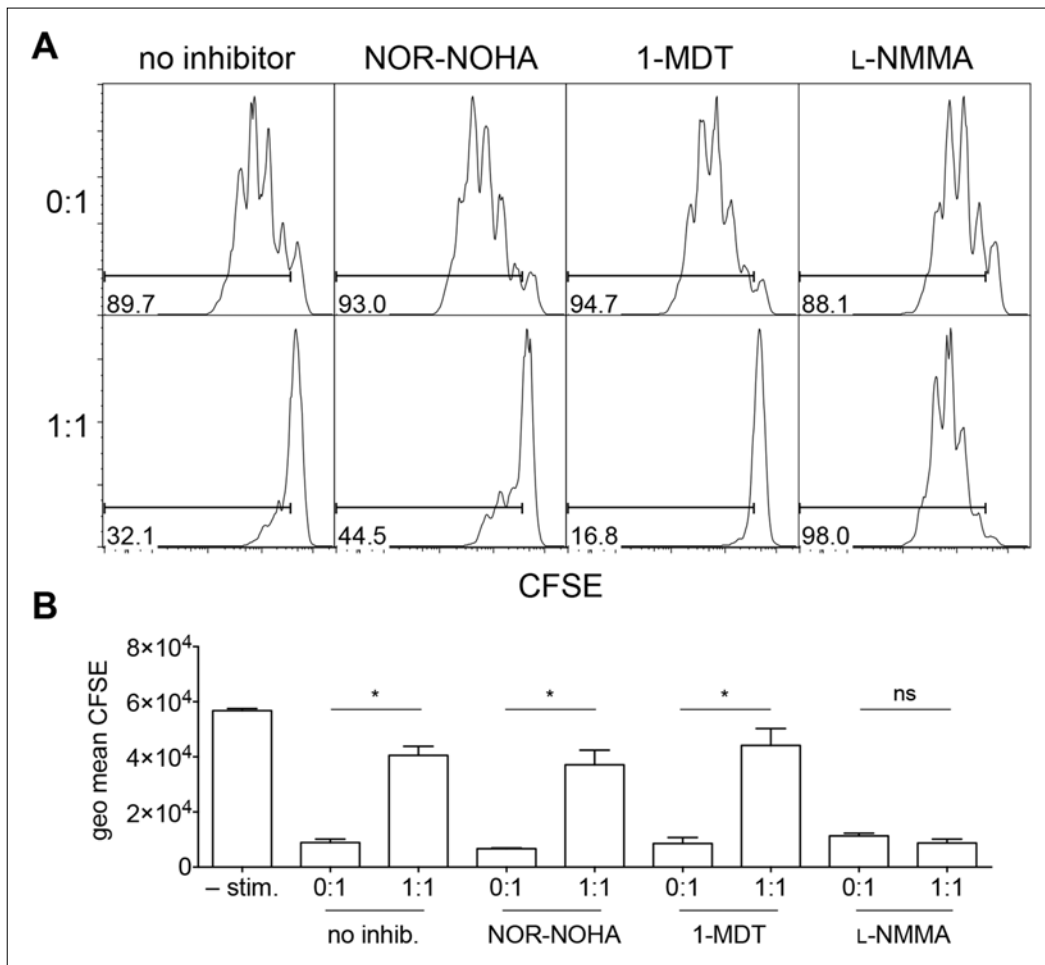
**Fig. 6.** Suppressive capacity of CD11b⁺Ly6C⁺⁺Ly6G⁻ cells from IAV-infected lungs relies on iNOS activity. (A) Naive CD4⁺ T cells were labeled with CFSE and stimulated for 4 days with plate-bound anti-CD3 and anti-CD28 antibodies in the absence (upper row) or presence (lower row) of CD11b⁺Ly6C⁺⁺Ly6G⁻ cells isolated from lungs of IAV-infected mice (day 6). Inhibitors against Arg1 (NOR-NOHA), IDO (1-MDT), and iNOS (L-NMMA) were added to both conditions or cells remained untreated (no inhibitor). At the end of the culture, cells were analyzed by flow cytometry. Histograms show CFSE profile of naive CD4⁺ T cells pregated as living CD4⁺CD11b⁻ cells. Numbers show frequency of cells that have lost CFSE. Each condition was performed in triplicates, and representative data from one out of two independently performed experiments are depicted. (B) Pooled geometric mean fluorescence intensity (geo mean) of CFSE in naive CD4⁺ T cells from the two experiments depicted in A (mean ± SD, $n = 6$). ns = not significant, * = $p \leq 0.05$, two-tailed unpaired $t$ test with Welch's correction

## Discussion

The results reported here present evidence that IAV infection induces the accumulation of CD11b⁺Ly6C⁺⁺Ly6G⁻ cells with the ability to use iNOS to suppress overwhelming immune responses. The study sheds new light on the role of infiltrating monocytes during IAV infection by indicating that monocyte-derived cells also perform anti-inflammatory functions in this context. Since the IFN-γ/iNOS axis was shown before to function as negative feedback regulator of inflammatory T cells [33], it is tempting to speculate that CD11b⁺Ly6C⁺⁺Ly6G⁻ cells and iNOS are involved in the self-limitation of the inflammatory response during IAV.

Many factors are involved in immune regulation during IAV infection. An elegant work showed that IL-10 production by virus-specific effector T cells is crucial to avoid immune-mediated lung disease and death in IAV-infected

mice [3]. Foxp3⁺ Treg cells also seem to be involved in the immune response to IAV, since an expansion of IAV-specific Foxp3⁺ Treg cells in lungs of infected mice was reported [4]. Despite the large number of immunosuppressive pathways during IAV infection, the virus can induce excessive lung inflammation under certain conditions. Lung infiltration by monocytes, for example, is considered detrimental for IAV-infected mice, as these cells were shown to differentiate *in situ* into TiP-DC and exert overwhelming proinflammatory functions [7–9]. In the present study, new evidence that lung-infiltrating monocytes might also exert an anti-inflammatory function, since they expressed different immunosuppressive genes and were able to suppress T cell proliferation *ex vivo*, was described. Most likely, monocyte-derived cells induce a proper T cell response upon IAV infection but, at the same time, evolve properties to avoid that this response becomes pathogenic. One explanation for the discrepancy – namely, the previously unrecognized anti-inflammatory role of lung-infil-

trating monocytes in IAV infection – might come from the fact that, by now, it is still difficult to distinguish between the progeny of infiltrating monocytes by means of surface markers and to study their function with *in vitro* functional assays. Future work on additional differentiation markers and standardized functional assays are needed to shed light on the progeny of lung-infiltrating monocytes in IAV infection. A promising approach might involve transcriptome-based network analysis, which was used recently for a systematic phenotypic and functional characterization of human and murine monocyte-derived macrophages upon activation [34]. The data on global transcriptional activity presented here might be useful for such future studies.

Interestingly, chemical or genetic blockade of iNOS improves resistance of mice to lethal IAV doses, which led to the conclusion that excessive iNOS expression and NO production are actually toxic and promote rather than prevent lung immunopathology in the IAV-infected lung [35–37]. In those studies, it was discussed whether production of NO, a highly toxic reactive nitrogen species, leads to destruction of delicate lung tissues. Our work indicates a new role of iNOS during IAV infection, namely, control of excessive T cell responses. However, this has to be further investigated since iNOS is expressed by only a very small subset of $CD11b^+Ly6C^{++}Ly6G^-$ cells within lungs of IAV-infected mice and since efficient inhibition of iNOS expression via *in vivo* IFN-γ-blockade at the peak of infection did not lead to changes in disease outcome. These data suggest that iNOS expression is only one pathway that can be used by $CD11b^+Ly6C^{++}Ly6G^-$ cells during IAV infection to avoid lung immunopathology. Indeed, we found that highly activated $CD11b^+Ly6C^{++}Ly6G^-$ cells in lungs of IAV-infected mice express a range of genes, which are associated with immunosuppression, including *Il10, Il27,* and *Vegfa* [3, 38, 39]. Therefore, our work, besides uncovering a new role for iNOS during IAV infection, also opens new questions on the specific role of the expression of these molecules by $CD11b^+Ly6C^{++}Ly6G^-$ cells in keeping immune balance during IAV infection.

In summary, monocyte-derived $CD11b^+Ly6C^{++}Ly6G^-$ cells were shown here to transiently accumulate in lungs of mice sublethally infected with IAV, where they become highly activated, expressing pro- and anti-inflammatory genes. The *in vitro* suppressive activity of $CD11b^+Ly6C^{++}Ly6G^-$ cells was dependent on iNOS, which is a new role for this molecule in the IAV infection model. Therefore, these observations might lead to a reconsideration of the role of monocytes and their progeny during IAV infection. Better understanding of immune regulation during IAV infection might result in the development of novel therapies to avoid immune-mediated lung damage and associated deaths.

## Acknowledgements

## Conflict of interest disclosure

The authors declare no financial or commercial conflict of interest.

## References

1. Cheung CY, Poon LL, Lau AS, Luk W, Lau YL, Shortridge KF, Gordon S, Guan Y, Peiris JS: Induction of proinflammatory cytokines in human macrophages by influenza A (H5N1) viruses: a mechanism for the unusual severity of human disease? Lancet 360, 1831–1837 (2002)

2. Kobasa D, Takada A, Shinya K, Hatta M, Halfmann P, Theriault S, Suzuki H, Nishimura H, Mitamura K, Sugaya N, Usui T, Murata T, Maeda Y, Watanabe S, Suresh M, Suzuki T, Suzuki Y, Feldmann H, Kawaoka Y: Enhanced virulence of influenza A viruses with the haemagglutinin of the 1918 pandemic virus. Nature 431, 703–707 (2004)

3. Sun J, Madan R, Karp CL, Braciale TJ: Effector T cells control lung inflammation during acute influenza virus infection by producing IL-10. Nat Med 15, 277–284 (2009)

4. Betts RJ, Prabhu N, Ho AW, Lew FC, Hutchinson PE, Rotzschke O, Macary PA, Kemeny DM: Influenza A virus infection results in a robust, antigen-responsive, and widely disseminated Foxp3+ regulatory T cell response. J Virol 86, 2817–2825 (2012)

5. Brincks EL, Roberts AD, Cookenham T, Sell S, Kohlmeier JE, Blackman MA, Woodland DL: Antigen-specific memory regulatory CD4+Foxp3+ T cells control memory responses to influenza virus infection. J Immunol 190, 3438–3446 (2013)

6. Moser EK, Hufford MM, Braciale TJ: Late engagement of CD86 after influenza virus clearance promotes recovery in a FoxP3+ regulatory T cell dependent manner. PLoS Pathog 10, e1004315 (2014)

7. Aldridge JR, Jr., Moseley CE, Boltz DA, Negovetich NJ, Reynolds C, Franks J, Brown SA, Doherty PC, Webster RG, Thomas PG: TNF/iNOS-producing dendritic cells are the necessary evil of lethal influenza virus infection. Proc Natl Acad Sci U S A 106, 5306–5311 (2009)

8. Lin KL, Suzuki Y, Nakano H, Ramsburg E, Gunn MD: CCR2+ monocyte-derived dendritic cells and exudate macrophages produce influenza-induced pulmonary immune pathology and mortality. J Immunol 180, 2562–2572 (2008)

9. Pamer EG: Tipping the balance in favor of protective immunity during influenza virus infection. Proc Natl Acad Sci U S A 106, 4961–4962 (2009)

10. Guilliams M, Lambrecht BN, Hammad H: Division of labor between lung dendritic cells and macrophages in the defense against pulmonary infections. Mucosal Immunol 6, 464–473 (2013)

11. Bronte V, Zanovello P: Regulation of immune responses by L-arginine metabolism. Nat Rev Immunol 5, 641–654 (2005)

12. Gabrilovich DI, Nagaraj S: Myeloid-derived suppressor cells as regulators of the immune system. Nat Rev Immunol 9, 162–174 (2009)

13. Nagaraj S, Gupta K, Pisarev V, Kinarsky L, Sherman S, Kang L, Herber DL, Schneck J, Gabrilovich DI: Altered recognition of antigen is a mechanism of CD8+ T cell tolerance in cancer. Nat Med 13, 828–835 (2007)

14. Munn DH, Shafizadeh E, Attwood JT, Bondarev I, Pashine A, Mellor AL: Inhibition of T cell proliferation by macrophage tryptophan catabolism. J Exp Med 189, 1363–1372 (1999)

15. Yu J, Du W, Yan F, Wang Y, Li H, Cao S, Yu W, Shen C, Liu J, Ren X: Myeloid-derived suppressor cells suppress antitumor immune responses through IDO expression and correlate with lymph node metastasis in patients with breast cancer. J Immunol 190, 3783–3797 (2013)

16. De Santo C, Salio M, Masri SH, Lee LY, Dong T, Speak AO, Porubsky S, Booth S, Veerapen N, Besra GS, Grone HJ, Platt FM, Zambon M, Cerundolo V: Invariant NKT cells reduce the immunosuppressive activity of influenza A virus-induced myeloid-derived suppressor cells in mice and humans. J Clin Invest 118, 4036–4048 (2008)

17. Wang J, Li F, Sun R, Gao X, Wei H, Li LJ, Tian Z: Bacterial colonization dampens influenza-mediated acute lung injury via induction of M2 alveolar macrophages. Nat Commun 4, 2106 (2013)

18. Blazejewska P, Koscinski L, Viegas N, Anhlan D, Ludwig S, Schughart K: Pathogenicity of different PR8 influenza A virus variants in mice is determined by both viral and host factors. Virology 412, 36–45 (2011)

19. Srivastava B, Blazejewska P, Hessmann M, Bruder D, Geffers R, Mauel S, Gruber AD, Schughart K: Host genetic background strongly influences the response to influenza a virus infections. PLoS One 4, e4857 (2009)

20. Kittel B, Ruehl-Fehlert C, Morawietz G, Klapwijk J, Elwell MR, Lenz B, O'Sullivan MG, Roth DR, Wadsworth PF: Revised guides for organ sampling and trimming in rats and mice – Part 2. A joint publication of the RITA and NACAD groups. Exp Toxicol Pathol 55, 413–431 (2004)

21. Bode J, Dutow P, Sommer K, Janik K, Glage S, Tummler B, Munder A, Laudeley R, Sachse KW, Klos A: A new role of the complement system: C3 provides protection in a mouse model of lung infection with intracellular Chlamydia psittaci. PLoS One 7, e50327 (2012)

22. Pruitt KD, Tatusova T, Maglott DR: NCBI reference sequences (RefSeq): a curated non-redundant sequence database of genomes, transcripts and proteins. Nucleic Acids Res 35, D61–65 (2007)

23. Anders S, Huber W: Differential expression analysis for sequence count data. Genome Biol 11, R106 (2010)

24. Battke F, Symons S, Nieselt K: Mayday – integrative analytics for expression data. BMC Bioinformatics 11, 121 (2010)

25. Maere S, Heymans K, Kuiper M: BiNGO: a Cytoscape plugin to assess overrepresentation of gene ontology categories in biological networks. Bioinformatics 21, 3448–3449 (2005)

26. Margolin AA, Wang K, Lim WK, Kustagi M, Nemenman I, Califano A: Reverse engineering cellular networks. Nat Protoc 1, 662–671 (2006)

27. Isserlin R, Merico D, Voisin V, Bader GD: Enrichment Map – a Cytoscape app to explore and visualize OMICs pathway enrichment results. F1000Res 3, 141 (2014)

28. Oesper L, Merico D, Isserlin R, Bader GD: WordCloud: a Cytoscape plugin to create a visual semantic summary of networks. Source Code Biol Med 6, 7 (2011)

29. Xie QW, Whisnant R, Nathan C: Promoter of the mouse gene encoding calcium-independent nitric oxide synthase confers inducibility by interferon gamma and bacterial lipopolysaccharide. J Exp Med 177, 1779–1784 (1993)

30. Griffith OW, Kilbourn RG: Nitric oxide synthase inhibitors: amino acids. Methods Enzymol 268, 375–392 (1996)

31. Tenu JP, Lepoivre M, Moali C, Brollo M, Mansuy D, Boucher JL: Effects of the new arginase inhibitor N(omega)-hydroxy-nor-L-arginine on NO synthase activity in murine macrophages. Nitric Oxide 3, 427–438 (1999)

32. Hou DY, Muller AJ, Sharma MD, DuHadaway J, Banerjee T, Johnson M, Mellor AL, Prendergast GC, Munn DH: Inhibition of indoleamine 2,3-dioxygenase in dendritic cells by stereoisomers of 1-methyl-tryptophan correlates with antitumor responses. Cancer Res 67, 792–801 (2007)

33. Feuerer M, Eulenburg K, Loddenkemper C, Hamann A, Huehn J: Self-limitation of Th1-mediated inflammation by IFN-gamma. J Immunol 176, 2857–2863 (2006)

34. Xue J, Schmidt SV, Sander J, Draffehn A, Krebs W, Quester I, De Nardo D, Gohel TD, Emde M, Schmidleithner L, Ganesan H, Nino-Castro A, Mallmann MR, Labzin L, Theis H, Kraut M, Beyer M, Latz E, Freeman TC, Ulas T, Schultze JL: Transcriptome-based network analysis reveals a spectrum model of human macrophage activation. Immunity 40, 274–288 (2014)

35. Akaike T, Noguchi Y, Ijiri S, Setoguchi K, Suga M, Zheng YM, Dietzschold B, Maeda H: Pathogenesis of influenza virus-induced pneumonia: involvement of both nitric oxide and oxygen radicals. Proc Natl Acad Sci U S A 93, 2448–2453 (1996)

36. Karupiah G, Chen JH, Mahalingam S, Nathan CF, MacMicking JD: Rapid interferon gamma-dependent clearance of influenza A virus and protection from consolidating pneumonitis in nitric oxide synthase 2-deficient mice. J Exp Med 188, 1541–1546 (1998)

37. Perrone LA, Belser JA, Wadford DA, Katz JM, Tumpey TM: Inducible nitric oxide contributes to viral pathogenesis following highly pathogenic influenza virus infection in mice. J Infect Dis 207, 1576–1584 (2013)

38. Liu FD, Kenngott EE, Schroter MF, Kuhl A, Jennrich S, Watzlawick R, Hoffmann U, Wolff T, Norley S, Scheffold A, Stumhofer JS, Saris CJ, Schwab JM, Hunter CA, Debes GF, Hamann A: Timed action of IL-27 protects from immunopathology while preserving defense in influenza. PLoS Pathog 10, e1004110 (2014)

39. Zanini A, Spanevello A, Baraldo S, Majori M, Della Patrona S, Gumiero F, Aiello M, Olivieri D, Saetta M, Chetta A: Decreased maturation of dendritic cells in the central airways of COPD patients is associated with VEGF, TGF-beta and vascularity. Respiration 87, 234–242 (2014)